Letter

Magnonic skin effect and magnon valve effect in an antiferromagnetically coupled heterojunction

Z. R. Yan,[1,2,*] Y. W. Xing,[1,*] and X. F. Han[1,2,3,†]

[1]*Beijing National Laboratory for Condensed Matter Physics, Institute of Physics, Chinese Academy of Sciences, Beijing 100190, China*
[2]*Center of Materials Science and Optoelectronics Engineering, University of Chinese Academy of Sciences, Beijing 100049, China*
[3]*Songshan Lake Materials Laboratory, Dongguan, Guangdong 523808, China*

(Received 2 February 2021; revised 20 April 2021; accepted 16 July 2021; published 30 July 2021)

We theoretically study the scattering behavior of spin waves (SWs) at the interface of an antiferromagnetically coupled (AFMC) heterojunction. It is shown that the SWs passing through the interface are evanescent and the incident waves are all reflected back, demonstrating a magnetization-dependent magnon blocking effect in this structure. We also analytically derive the expressions for the decay length of the evanescent waves (EWs). The theoretical result indicates that with the increase of the spin-wave (SW) frequency, the decay length decreases and the EWs are more concentrated at the interface, showing a magnonic skin effect (MSE) which is similar to the skin effect of electromagnetic waves. Furthermore, a positive magnonic Goos-Hänchen shift (MGHS) of the reflected waves is also predicted. It can be understood by an effective reflection interface shift induced by the nonzero decay length of the EWs. The results of micromagnetic simulations are consistent well with all the theoretical findings. Based on the above findings, we also propose a magnon valve without spacers, which shows 100% on-off ratio for magnons. Our work provides insights into SW transmissions in the system of AFMC heterostructures and will serve as a promising tool for future magnonic devices.

DOI: 10.1103/PhysRevB.104.L020413

Spin waves (SWs) or magnons, the eigenexcitations of the electron spin subsystem in magnetically ordered media, are promising data carriers in next-generation information processing devices [1–3]. The crucial advantage of magnonic devices is free of charge currents and thus excluding Ohmic losses [4]. It enables the magnonic units to supplement or even replace charge-based complementary metal-oxide semiconductor (CMOS) circuits [2]. Recently, plenty of magnonic devices are theoretically proposed and experimentally reported, such as various magnon transistors [5–11] and spin-wave (SW) logic gates [12–19]. In these applications, SWs are usually used as information carriers transferring from one medium (region) to another. Thus, the detailed knowledge about the scattering behaviors of SWs at the interface between two media (regions) is crucial.

In recent years, with the improvement of experimental techniques and capability of computers, the SW scattering at the interfaces become a hot topic and various interfaces are noticed and studied, such as the domain wall boundary [20–25], the edge of inhomogeneous DMI [26–29] or magnetic field [30,31], and the interface between two ferromagnets [32,33]. Numerous remarkable phenomena related to these interfaces are reported. For example, the magnonic Goos-Hänchen shift (MGHS)—as the magnetic analog of the optical Goos-Hänchen effect—represents a lateral shift along the interface between the incident and reflected (or transmitted) SW beam spots, is finally confirmed by the experiments [34] after 35 years of its prediction [35]. Other classical optical effects, such as Snell's law [24,26,27,36], Mirage effect [31], and the negative refraction [20], can also occur in the SW systems with specific boundaries. Based on these significant findings, some designs and proposals are theoretically reported such as SW fibers [24,31], SW diodes [23], and so on. Recently, an experimental result shows a synthetic antiferromagnet without spacers [37,38]. It suggests that a new type of interface of an antiferromagnetically coupled (AFMC) heterojunction can be constructed. Nonetheless, the SW scattering at this interface has not yet been extensively explored.

To theoretically investigate this issue, we consider a system of two semi-infinite ferrimagnetic insulators (FMI_1 and FMI_2) with antiferromagnetic coupling at the interface as shown in Fig. 1(a). The magnetization configuration of two FMIs is antiparallel at zero applied magnetic field [37,38]. We assume a small fluctuation of the unit magnetization vector $\mathbf{m}_\eta$ of FMI_η ($\eta = 1$ or 2) around $\mathbf{m}_{0,\eta}$, (with $\mathbf{m}_{0,1} = +\mathbf{e}_z$ and $\mathbf{m}_{0,2} = -\mathbf{e}_z$) as $\mathbf{m}_\eta = \mathbf{m}_{0,\eta} + \delta\mathbf{m}_\eta$ with $\delta\mathbf{m}_\eta = (m_{x,\eta}, m_{y,\eta}, 0)$ and $|\delta\mathbf{m}_\eta| \ll 1$. The magnetic dynamics are described by the Landau-Lifshitz-Gilbert (LLG) equation [39],

$$\frac{\partial \mathbf{m}_\eta}{\partial t} = -\gamma \mathbf{m}_\eta \times \mathbf{H}_\eta^{\text{eff}} + \alpha \mathbf{m}_\eta \times \frac{\partial \mathbf{m}_\eta}{\partial t}, \tag{1}$$

where γ is the gyromagnetic ratio, α is the Gilbert damping constant. $\mathbf{H}_\eta^{\text{eff}} = \sigma_\eta(\frac{2K_\eta}{M_\eta}\hat{e}_z + \frac{A_\eta}{M_\eta}\nabla^2\mathbf{m}_\eta)$ is the effective field with saturation magnetization M_η, the exchange stiffness constant A_η, and the uniaxial magnetic anisotropy constant K_η of FMI_η. $\sigma_1 = +1$ and $\sigma_2 = -1$ are the orientation factors stemming from the magnetization parallel and antiparallel to the z axis. This work mainly investigates the exchange dominated

*These authors contributed equally to this work.
†Corresponding author: xfhan@iphy.ac.cn

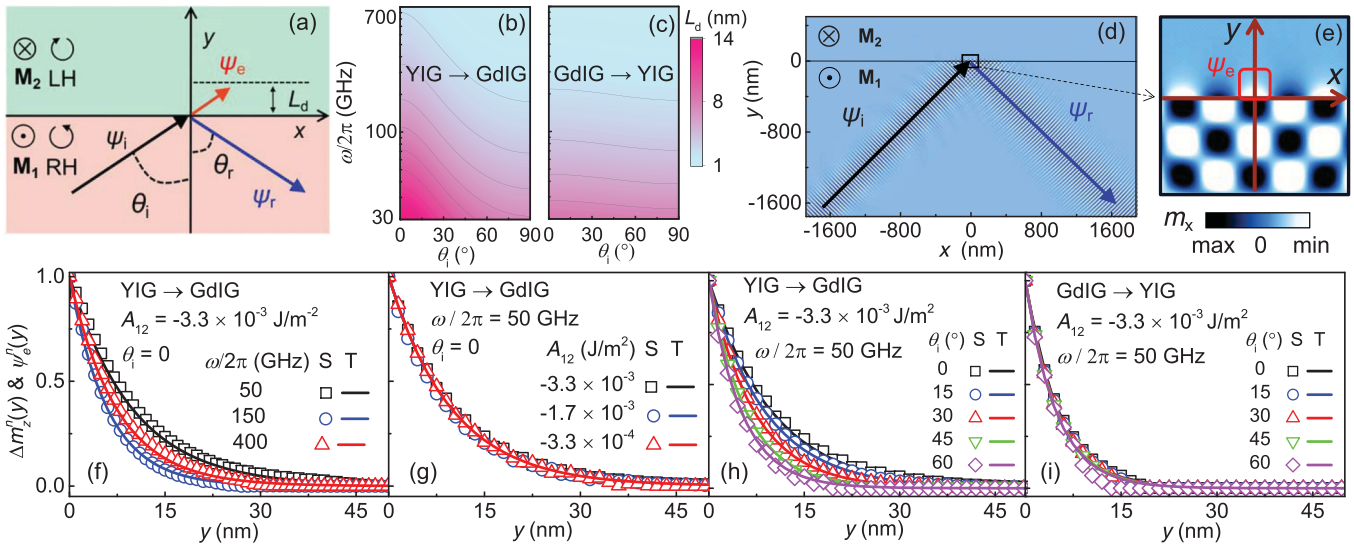

FIG. 1. An AFMC FMI bilayer and space dependence of the evanescent SW beam. (a) Illustration of the SW scattering at the interface of bilayer. Bottom layer is FMI_1 whose magnetization is along the direction of the $+z$ axis ($\odot$) accommodating right-handed polarized (RH, $\circlearrowleft$) SWs, and magnetization of FMI_2 in the top layer is along z-axis direction ($\otimes$) accommodating left-handed polarized (LH, $\circlearrowright$) SWs. Black, blue, and red arrows indicate the propagating direction of the injected SWs beam ψ_i, reflected SWs beam ψ_r, and evanescent SWs beam ψ_e. L_d is the decay length of $|\psi_e|$. L_d under various frequency ω and incident angles θ_i for (b) SWs injected from YIG into GdIG (YIG $\rightarrow$ GdIG) and (c) GdIG into YIG (GdIG $\rightarrow$ YIG). (d) Intensity map obtained from micromagnetic simulation of SW scattering at the interface of FMI bilayer. (e) The partial enlarged detail of the interface as marked by the black square in (d). The evanescent SW beam ψ_e is marked by the red square. Analytical and simulated $\psi_e(y)$ at (f) various ω for YIG $\rightarrow$ GdIG, $\theta_i = 0$, and $A_{12} = -3.3 \times 10^{-3}$ J/m^2, (g) various A_{12} for YIG $\rightarrow$ GdIG, $\theta_i = 0$, and $\omega/2\pi = 50$ GHz, (h) various θ_i for YIG $\rightarrow$ GdIG, $A_{12} = -3.3 \times 10^{-3}$ J/m^2, and $\omega/2\pi = 50$ GHz, and (i) various θ_i for GdIG $\rightarrow$ YIG, $A_{12} = -3.3 \times 10^{-3}$ J/m^2, and $\omega/2\pi = 50$ GHz. The empty symbols represent the results of simulations (S) and solid lines for the results of theory (T).

magnon with high frequency, and thus the influence of dipolar field can be ignored (for details, see the Supplemental Material [40]). This simplification does not affect the reliability of results in high frequency region, which has been proved by previous works [11,23,24,28,41–43]. Considering a negligible α and defining a SW function $\psi_\eta = m_{x,\eta} - im_{y,\eta}$, effective Schrödinger equations can be deduced from the Eq. (1) [21]:

$$i\hbar\frac{\partial\Phi_\eta}{\partial t} = \mathcal{H}_\eta\Phi_\eta = \left[\frac{\hat{p}^2}{2m_\eta^*} + V_\eta\right]\Phi_\eta, \tag{2}$$

where $\hat{p} = -i\hbar\nabla$ is the momentum operator, $m_\eta^* = \hbar\sigma_\eta A_\eta/4\gamma M_\eta$ is the effective mass of magnons, and $V_\eta = 2\gamma\hbar\sigma_\eta K_\eta/M_\eta$ is the potential energy. The plane wave function of $\Phi_\eta \sim e^{i(\mathbf{k}\cdot\mathbf{r}-\omega_\eta t)}$ is a general solution of Eq. (2) and the energy of FMI_η layer can be obtained as $E_\eta = \hbar\omega_\eta = \frac{k^2}{2m_\eta^*} + V_\eta = \hbar\gamma\sigma_\eta M_\eta(2A_\eta k_\eta^2 + 2K_\eta)$. It is noted that positive (negative) SW frequency ω_η indicates right-handed (left-handed) polarized [RP (LP)] wave feature [10,44].

For the SW scattering at the interface of the bilayer, an incident SW beam ψ_i with an incident angle θ_i, a reflected beam ψ_r with a reflected angle θ_r in FMI_1, and a transmitted beam ψ_e in FMI_2 are naturally considered. The ψ_e is an evanescent wave (EW) which will be discussed in detail later. Thus, the SWs in FMI_1 and FMI_2 can be assumed as $\Phi_1(x,y) = \psi_i + \psi_r = e^{i(k_x^i x + k_y^i y)} + Re^{i(k_x^r x + k_y^r y)}$ and $\Phi_2(x,y) = \psi_e = Te^{i(k_x^e x + k_y^e y)}$. The tangential component of the wave vector at the interface is conserved, $k_x^i = k_x^r = k_x^e$ because of the translational symmetry, and $k_y^i = -k_y^r$ due to law of reflection $\theta_i = \theta_r$. The k_y^e of the transmitted waves can be obtained by solving stationary Schrödinger equation in FMI_2 $\mathcal{H}_2\Phi_2 = E\Phi_2$, where $E = \hbar\omega$ is energy of the incident SWs. Thus, the k_y^e of the transmitted waves can be obtained as

$$k_y^e = i\sqrt{\frac{\left(\frac{\omega M_2}{\gamma} + 2K_2\right)}{2A_2} + \sin^2(\theta_i)\frac{\left(\frac{\omega M_1}{\gamma} - 2K_1\right)}{2A_1}}, \tag{3}$$

k_y^e is a pure imaginary number, indicating ψ_e is an EW whose decay length is $L_d = 1/|k_y^e|$. The reflection coefficients R can be obtained by solving the Hoffmann boundary condition [45,46]: $A_1\frac{\partial\Phi_1}{\partial y} - A_{12}[\Phi_1 + \Phi_2] = 0$ and $A_2\frac{\partial(-\Phi_2)}{\partial y} - A_{12}[\Phi_1 + \Phi_2] = 0$, where $A_{12} < 0$ is the interfacial AFMC constant between FMI_1 and FMI_2. The negative sign of Φ_2 originates from the orientation of M_2 antiparallel to the z axis. The AFMC YIG|GdIG bilayer [37] is investigated and the material-related parameters are as follows. The saturation magnetization, the exchange stiffness constant, and the uniaxial magnetic anisotropy constants are $M_1 = 1.5 \times 10^5$ A/m, $A_1 = 3.6 \times 10^{-12}$ J/m, $K_1 = 10$ J/m^3 for YIG [47–49] and $M_2 = 0.3 \times 10^5$ A/m, $A_2 = 3 \times 10^{-12}$ J/m, $K_2 = 4000$ J/m^3 for GdIG [49,50]. Therefore, the reflection coefficients are written as $R = \frac{A_1A_{12}k_y^i - A_2A_{12}k_y^e + iA_1A_2k_y^ik_y^e}{A_1A_{12}k_y^i + A_2A_{12}k_y^e + iA_1A_2k_y^ik_y^e}$. It is obvious that $|R|^2$ is equal to 1, demonstrating a total reflection of the incident SWs, which can be explained by the magnetization-dependent magnon blocking effect as reported by our previous work [10]. It is found that a system with effective ferromagnetic interfacial coupling and strong magnetic anisotropy can also

lead to 100% SW reflection at the antiparallel interface [51], indicating that the so-called magnon blocking effect is universal in the antiparallel systems with no matter ferromagnetic or antiferromagnetic interfacial coupling. On the other hand, some previous work reported that the large transmission of spin waves can be caused by the domain wall with a large width [51–53], indicating that only the antiparallel system with a sharply changed interface can lead to the total reflection. In our work, an effective domain wall with ultranarrow width is introduced between two FMIs, suppressing the transmission of spin waves. Besides, the MGHS of the reflected SW beam can be deduced by formula $L_{\mathrm{GH}} = -\partial \arctan[\frac{\mathrm{Im}(R)}{\mathrm{Re}(R)}]/\partial k_x$ [28,33,54] where $\mathrm{Im}(R)$ and $\mathrm{Re}(R)$ are the imaginary and real parts of the reflection coefficient, respectively.

We first investigate the L_{d} of the EWs (or called penetration depth of incident waves). The phase diagrams with contours of L_{d} as a function of the incident angle θ_i and frequency ω are shown in Figs. 1(b) and 1(c). It is obvious that L_{d} is inversely proportional to θ_i. The reason is that the increase of θ_i leads to the decrease of the normal component of the momentum k_y, and further results in suppressing the diffusing of SWs. Therefore, when SWs are normal incident ($\theta_i = 0$), L_{d} has the maximum value. Besides, the L_{d}- θ_i functions depend on the paths of the SW beams, i.e., transmitting from YIG to GdIG or vice versa. As the θ_i increases, the L_{d} decreases more quickly from YIG to GdIG than GdIG to YIG. In Figs. 1(b) and 1(c) the relations between L_{d} and ω are also appealing. The decrease of L_{d} with the increase of ω shows that the SWs with higher frequency decay more quickly, leading to the concentration of the EWs at the interface, which is called a magnonic skin effect (MSE). This phenomenon is similar to the skin effect in electrodynamics which describes that the electromagnetic waves transmitted from air to a conductor will have the smaller decay lengths when the frequency increases [55,56]. The MSE can be understood by the following mechanism. The polarization of the EWs is RP as the same as the incident waves, however FMI_2 is a medium of LP waves, suggesting that the propagating of the EWs is based on the forced reversed precession of spin in FMI_2. With the increase of ω, the forced reversed precession become harder, leading to the decrease of L_{d}.

GPU-accelerated micromagnetic simulation framework (Mumax3) [57] was used to verify the theoretical predictions. An example result is shown in Fig. 1(d). The incident SW beam ψ_i and reflected SW beam ψ_r are marked by black and blue arrows while the EW ψ_e is shown as a black square which is also shown in an enlarged version in Fig. 1(e). Based on $\psi_e = m_x - im_y$, one can find $|\psi_e(\mathbf{r})| = \sqrt{m_x^2(\mathbf{r}) + m_y^2(\mathbf{r})} = \sqrt{1 - m_z^2(\mathbf{r})} = \Delta m_z(\mathbf{r})$. Thus, the space-dependent reduction of z component of normalized magnetization $\Delta m_z^n(y) = \Delta m_z(y)/\Delta m_z(0)$ can be calculated for comparing with the normalized EW $|\psi_e^n(y)| = |\psi_e(y)|/|\psi_e(0)|$ of theoretical prediction. Figure 1(f) shows $\Delta m_z^n(y)$ and $|\psi_e^n(y)|$ for various ω at $\theta_i = 0$ and $A_{12} = -3.3 \times 10^{-3}$ J/m^2. By increasing the frequency of the incident SWs, ω, $\Delta m_z^n(y)$, and $|\psi_e^n(y)|$ declines more rapidly, indicating the decrease of L_{d} as marked by the dashed lines. These simulation results have confirmed the MSE. Besides, the influences of A_{12} are shown in Fig. 1(g).

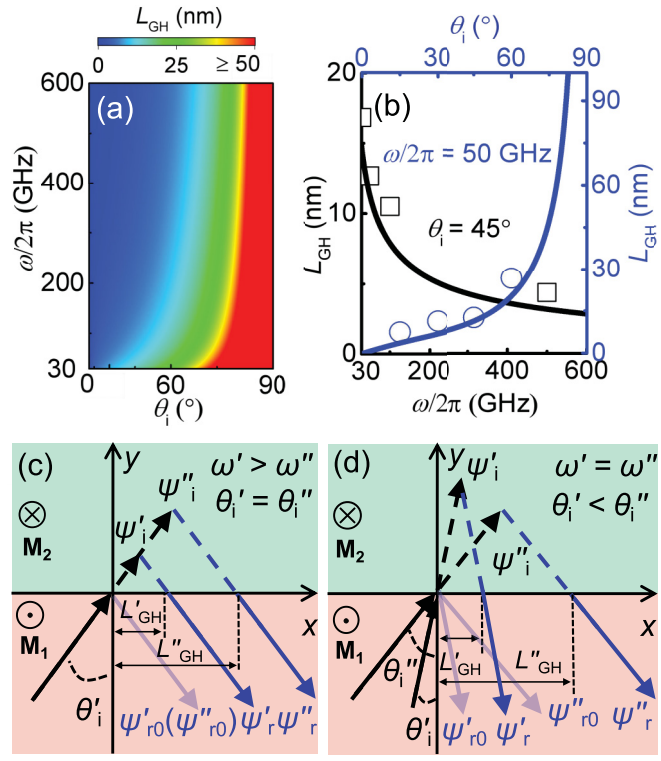

FIG. 2. Magnonic Goos-Hänchen shift at heterochiral interfaces. (a) Phase diagram of L_{GH} under various ω and θ_i. (b) Analytical and simulated L_{GH} of MGHS at $\theta_i = 45^\circ$ and $\omega/2\pi = 50$ GHz. Schematic plot of the MGHS under (c) different frequency ω and (d) incident angles θ_i.

For $\Delta m_z^n(y)$ with different A_{12}, they coincide totally, indicating that A_{12} is not important for the decay process of the EWs. Figures 1(h) and 1(i) show the results of the EWs with various θ_i. The EWs decay more sharply as the increase of θ_i, showing that L_{d} is inversely proportional to θ_i as pointed by the theory. Furthermore, the simulation results also reproduce the noncommutation of the EWs between the cases of YIG → GdIG and GdIG → YIG. In our simulation, the size of mesh and simulation time step is not small enough and the amplitudes of some EWs are weak, leading to the sizable fitting error between symbols and curves.

Then we investigate the MGHS of the reflected SW beams. According to the analytical solution of L_{GH}, we plot the phase diagram of the MGHS as a function of the incident angle θ_i and the frequency ω as shown in Fig. 2(a). First, it is noticed that the symbol of L_{GH} is positive, showing a positive shift between the reflected and incident spot. It can be understood by the effective shift of reflection interface as shown in Figs. 2(c) and 2(d). In other words, the incident wave can penetrate into the other layer and thus the scattering of SWs occurs above the surface at $y = 0$. Due to the effective scattering interface at $y > 0$, the SWs have a nonzero propagation path along x axis, resulting in a positive MGHS of reflected SW beams. For two different incident waves ψ'_i and ψ''_i, which have the same incident angle ($\theta'_i = \theta''_i$) but different frequency ($\omega' > \omega''$) [Fig. 2(c)], due to that higher frequency leads to smaller L_{d}, i.e., the smaller penetration

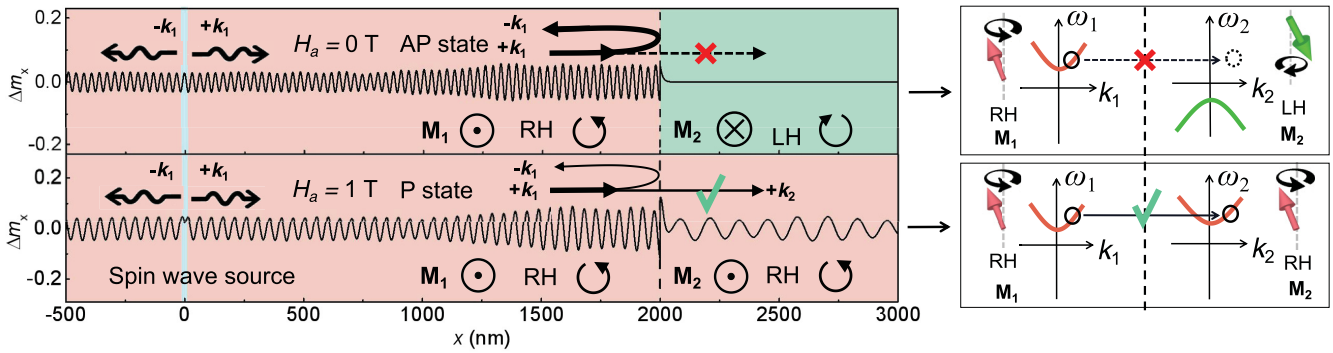

FIG. 3. The proposed magnon valve and simulated magnon transmission. The forward-propagating SWs and backward-propagating SWs can be excited by a SW source which is set in $x = 0$ nm. The interface between two coupled magnetic layers is at $x = 2000$ nm. Red region represents magnetization along $+z$ direction and green region for magnetization along $+z$ direction. Under large applied field ($H_a = 1$ T), the magnetization state of both layers is parallel (P). Under zero applied field ($H_a = 0$ T), they are antiparallel (AP) state. The collective excitations of the upward (⊙) and downward (⊗) magnetic order in simple ferromagnets, which are marked by red and green regions, correspond to different spin-wave dispersion relation of the ω-k function, suggesting that they can only excite right-handed polarization (RH, ↻) or left-handed polarization (LH, ↺) of spin waves, respectively. For AP state, the magnon with ↻ modes exited from M_1 (⊙) region are in the forbidden band of M_2 (⊗) region, suppressing the transmission from M_1 (⊙) to M_2 (⊗). For P state, both region are ⊙, so magnon with ↻ modes exited from M_1 (⊙) region are in the pass band of M_2 (⊙) region, allowing the magnon transmission between two regions.

depth of the incident waves, the propagation path along x axis become shorter, leading to a smaller MGHS ($L'_{\mathrm{GH}} < L''_{\mathrm{GH}}$). For two different incident waves which have the same frequency ($\omega' = \omega''$) but different incident angle ($\theta'_i < \theta''_i$) [Fig. 2(d)], the larger incident angle directly enhances k_x^e, which causes a longer propagation path along x axis. As a result, the MGHS become larger ($L'_{\mathrm{GH}} < L''_{\mathrm{GH}}$). The micromagnetic simulation results are shown in Fig. 2(b) and well consistent with the theoretical predictions, confirming the validity of the above physical mechanism.

Based on the above results, we therefore proposed a magnon valve (MV) device which can be used for manipulating the magnon transmission. In recent years, the magnon valve effect (MVE) was reported in various MV systems, opening a door for promising applications in magnon spintronics. One of classical MV devices were constructed by FMI/spacer (nonmagnetic metal or antiferromagnetic insulator)/FMI sandwiches [7,8], where the magnon transmission is spin dependent and this phenomenon is called MVE. In these systems, MVE can be explained by that when the magnetization of the two FMI layers is parallel (antiparallel), the total magnon current is additive (subtractive), leading to different output signals of magnon [58]. In the FMI/antiferromagnetic insulator/FMI based MV devices, the magnon blocking effect was discovered and therefore an in-plane type of MV was proposed [10]. Besides, a new type of MV device, magnonic-crystal-based MV, was theoretically proposed recently, showing a MVE which is based on transmission spectra shift effect between up and down states of magnetization [11]. In spite of much previous effort, MVE with 100% on-off ratio of magnon currents is still not easy to be realized. We have noticed that some previous works reported the large transmission coefficients T of SWs (nearly equal to 1) in FMI bilayer system where magnetization configuration is parallel (P) [33]. It motivated us to design a MV with the AFMC FMI bilayer structure such as YIG|GdIG and the simulated SW propagation in AP and P state is shown in Fig. 3. It is shown that at large applied field the magnetization configuration of YIG and GdIG is P, showing a large T. As a contrast, for zero applied field, the configuration of bilayer is AP, leading to total reflection of SWs, i.e., $T = 0$, due to that different polarizations accommodate different magnon spin. The basic mechanism in MVE of this device is discussed in the notes of Fig. 3. Based on these proofs, a MV without spacers and with 100% on-off ratio of magnon currents is possible to be realized, which arouses a promising direction for designing new type of MVs.

In summary, we have investigated the SW scattering behavior at the interface of an AFMC FMI bilayer by theory and micromagnetic simulations. As for SWs injected from FMI_1 to FMI_2, we found a total reflection at the interface. It stemmed from a magnetization-dependent magnon blocking effect as reported by previous work. Furthermore, MSE was found and it showed that the higher-frequency waves with shorter decay lengths are more concentrated at the interface. Besides, the MGHS of the reflected waves was also investigated. It can be understood by a shift of the effective scattering interface induced by the finite penetration depth of the incident waves. The results of micromagnetic simulations are qualitatively and quantificationally consistent with the theoretical findings. Finally, we propose a magnon valve without spacers, which shows 100% magnonic on-off ratio. Our work sheds new light on both the fundamental physics and the appealing application of SW devices.

This work was supported by the National Key Research and Development Program of China (MOST, Grants No. 2017YFA0206200 and No. 2016YFA0300802), the National Natural Science Foundation of China (NSFC, Grants No. 51831012, and No. 51620105004), Beijing Natural Science Foundation (Grant No. Z201100004220006), and partially supported by the Strategic Priority Research Program (B) (Grant No. XDB33000000) of the Chinese Academy of Sciences (CAS).

[1] A. Serga, A. Chumak, and B. Hillebrands, J. Phys. D **43**, 264002 (2010).
[2] A. V. Chumak, V. I. Vasyuchka, A. A. Serga, and B. Hillebrands, Nat. Phys. **11**, 453 (2015).
[3] A. Chumak, A. Serga, and B. Hillebrands, J. Phys. D **50**, 244001 (2017).
[4] S. Neusser and D. Grundler, Adv. Mater. **21**, 2927 (2009).
[5] A. V. Chumak, A. A. Serga, and B. Hillebrands, Nat. Commun. **5**, 4700 (2014).
[6] J. Cramer, F. Fuhrmann, U. Ritzmann, V. Gall, T. Niizeki, R. Ramos, Z. Qiu, D. Hou, T. Kikkawa, J. Sinova, U. Nowak, E. Saitoh, and M. Kläui, Nat. Commun. **9**, 1089 (2018).
[7] H. Wu, L. Huang, C. Fang, B. S. Yang, C. H. Wan, G. Q. Yu, J. F. Feng, H. X. Wei, and X. F. Han, Phys. Rev. Lett. **120**, 097205 (2018).
[8] C. Y. Guo, C. H. Wan, X. Wang, C. Fang, P. Tang, W. J. Kong, M. K. Zhao, L. N. Jiang, B. S. Tao, G. Q. Yu, and X. F. Han, Phys. Rev. B **98**, 134426 (2018).
[9] P. Tang and X. F. Han, Phys. Rev. B **99**, 054401 (2019).
[10] Z. R. Yan, C. H. Wan, and X. F. Han, Phys. Rev. Appl. **14**, 044053 (2020).
[11] Y. W. Xing, Z. R. Yan, and X. F. Han, Phys. Rev. B **103**, 054425 (2021).
[12] M. Kostylev, A. Serga, T. Schneider, B. Leven, and B. Hillebrands, Appl. Phys. Lett. **87**, 153501 (2005).
[13] T. Schneider, A. A. Serga, B. Leven, B. Hillebrands, R. L. Stamps, and M. P. Kostylev, Appl. Phys. Lett. **92**, 022505 (2008).
[14] M. Jamali, J. H. Kwon, S.-M. Seo, K.-J. Lee, and H. Yang, Sci. Rep. **3**, 3160 (2013).
[15] K. Vogt, F. Y. Fradin, J. E. Pearson, T. Sebastian, S. D. Bader, B. Hillebrands, A. Hoffmann, and H. Schultheiss, Nat. Commun. **5**, 3727 (2014).
[16] A. A. Nikitin, A. B. Ustinov, A. A. Semenov, A. V. Chumak, A. A. Serga, V. I. Vasyuchka, E. Lähderanta, B. A. Kalinikos, and B. Hillebrands, Appl. Phys. Lett. **106**, 102405 (2015).
[17] K. Wagner, A. Kákay, K. Schultheiss, A. Henschke, T. Sebastian, and H. Schultheiss, Nat. Nanotechnol. **11**, 432 (2016).
[18] B. Rana and Y. C. Otani, Phys. Rev. Appl. **9**, 014033 (2018).
[19] W. Yu, J. Lan, and J. Xiao, Phys. Rev. Appl. **13**, 024055 (2020).
[20] S.-K. Kim, S. Choi, K.-S. Lee, D.-S. Han, D.-E. Jung, and Y.-S. Choi, Appl. Phys. Lett. **92**, 212501 (2008).
[21] P. Yan, X. S. Wang, and X. R. Wang, Phys. Rev. Lett. **107**, 177207 (2011).
[22] X.-g. Wang, G.-h. Guo, Y.-z. Nie, G.-f. Zhang, and Z.-x. Li, Phys. Rev. B **86**, 054445 (2012).
[23] J. Lan, W. Yu, R. Wu, and J. Xiao, Phys. Rev. X **5**, 041049 (2015).
[24] W. Yu, J. Lan, R. Wu, and J. Xiao, Phys. Rev. B **94**, 140410(R) (2016).
[25] J. Han, P. Zhang, J. T. Hou, S. A. Siddiqui, and L. Liu, Science **366**, 1121 (2019).
[26] J. Mulkers, B. Van Waeyenberge, and M. V. Milošević, Phys. Rev. B **97**, 104422 (2018).
[27] Z. Wang, B. Zhang, Y. Cao, and P. Yan, Phys. Rev. Appl. **10**, 054018 (2018).
[28] Z. Wang, Y. Cao, and P. Yan, Phys. Rev. B **100**, 064421 (2019).
[29] S.-J. Lee, D.-K. Lee, and K.-J. Lee, Phys. Rev. B **101**, 064422 (2020).
[30] J. Jorzick, S. O. Demokritov, B. Hillebrands, M. Bailleul, C. Fermon, K. Y. Guslienko, A. N. Slavin, D. V. Berkov, and N. L. Gorn, Phys. Rev. Lett. **88**, 047204 (2002).
[31] P. Gruszecki and M. Krawczyk, Phys. Rev. B **97**, 094424 (2018).
[32] Y. S. Dadoenkova, N. Dadoenkova, I. Lyubchanskii, M. Sokolovskyy, J. W. Kłos, J. Romero-Vivas, and M. Krawczyk, Appl. Phys. Lett. **101**, 042404 (2012).
[33] P. Gruszecki, M. Mailyan, O. Gorobets, and M. Krawczyk, Phys. Rev. B **95**, 014421 (2017).
[34] J. Stigloher, T. Taniguchi, H. S. Körner, M. Decker, T. Moriyama, T. Ono, and C. H. Back, Phys. Rev. Lett. **121**, 137201 (2018).
[35] K. Yasumoto and Y. Ōishi, J. Appl. Phys. **54**, 2170 (1983).
[36] J. Stigloher, M. Decker, H. S. Körner, K. Tanabe, T. Moriyama, T. Taniguchi, H. Hata, M. Madami, G. Gubbiotti, K. Kobayashi *et al.*, Phys. Rev. Lett. **117**, 037204 (2016).
[37] J. M. Gomez-Perez, S. Vélez, L. McKenzie-Sell, M. Amado, J. Herrero-Martín, J. López-López, S. Blanco-Canosa, L. E. Hueso, A. Chuvilin, J. W. A. Robinson, and F. Casanova, Phys. Rev. Appl. **10**, 044046 (2018).
[38] L. Wang, Z. Lu, X. Zhao, W. Zhang, Y. Chen, Y. Tian, S. Yan, L. Bai, and M. Harder, Phys. Rev. B **102**, 144428 (2020).
[39] T. L. Gilbert, IEEE Trans, Magn. **40**, 3443 (2004).
[40] See Supplemental Material at http://link.aps.org/supplemental/10.1103/PhysRevB.104.L020413 for analysis of ignoring dipole-dipole interaction, which includes Refs. [11,23,24,28,41–43].
[41] S.-J. Lee, J.-H. Moon, H.-W. Lee, and K.-J. Lee, Phys. Rev. B **96**, 184433 (2017).
[42] B. Lenk, H. Ulrichs, F. Garbs, and M. Münzenberg, Phys. Rep. **507**, 107 (2011).
[43] B. Kalinikos and A. Slavin, J. Phys. C: Solid State Phys. **19**, 7013 (1986).
[44] Z. W. Zhou, X. G. Wang, Y. Z. Nie, Q. L. Xia, Z. M. Zeng, and G. H. Guo, Phys. Rev. B **99**, 014420 (2019).
[45] F. Hoffmann, Phys. Status Solidi B **41**, 807 (1970).
[46] F. Hoffmann, A. Stankoff, and H. Pascard, J. Appl. Phys. **41**, 1022 (1970).
[47] J. Xiao and G. E. W. Bauer, Phys. Rev. Lett. **108**, 217204 (2012).
[48] S. Klingler, A. V. Chumak, T. Mewes, B. Khodadadi, C. Mewes, C. Dubs, O. Surzhenko, B. Hillebrands, and A. Conca, J. Phys. D: Appl. Phys. **48**, 015001 (2014).
[49] M. Althammer, J. Phys. D: Appl. Phys. **51**, 313001 (2018).
[50] H. Lassri, E. Hlil, S. Prasad, and R. Krishnan, J. Solid State Chem. **184**, 3216 (2011).
[51] P. Yan and G. E. W. Bauer, Phys. Rev. Lett. **109**, 087202 (2012).
[52] S. Macke and D. Goll, J. Phys. Conf. Ser **200**, 042015 (2010).
[53] C. Bayer, H. Schultheiss, B. Hillebrands, and R. Stamps, IEEE Trans. Magn. **41**, 3094 (2005).
[54] K. Artmann, Ann. Phys. (Berlin) **437**, 87 (1948).
[55] J. Schoenwald, E. Burstein, and J. Elson, Solid State Commun. **12**, 185 (1973).
[56] D. Begley, R. Alexander, C. Ward, R. Miller, and R. Bell, Surf. Sci. **81**, 245 (1979).
[57] A. Vansteenkiste, J. Leliaert, M. Dvornik, M. Helsen, F. Garcia-Sanchez, and B. Van Waeyenberge, AIP Adv. **4**, 107133 (2014).
[58] Y. Cheng, K. Chen, and S. Zhang, Appl. Phys. Lett. **112**, 052405 (2018).